Journal of the European Ceramic Society 20 (2000) 1603–1609

Applicability of the brick layer model to describe the grain boundary properties of strontium titanate ceramics

J.C.C. Abrantes [a], J.A. Labrincha [b], J.R. Frade [b,*]

[a] *ESTG, Instituto Politécnico de Viana do Castelo, Ap. 574, 4900 Viana do Castelo, Portugal*
[b] *Ceramics and Glass Engineering Department (UIMC), University of Aveiro, 3810 Aveiro, Portugal*

Received 27 July 1999; received in revised form 25 October 1999; accepted 8 November 1999

Abstract

Impedance spectroscopy was used to evaluate the bulk and grain boundary resistances (R_B and R_{gb}) of undoped strontium titanate ceramics in air and in N_2. The high frequency contribution of the spectra does not depend significantly on the average grain size or grain size distributions, and was thus ascribed to the bulk behaviour. The grain boundary results obtained for several samples vary with the average grain size, and these effects nearly agree with predictions by a simple brick layer model. The deviations from this model may increase with decreasing temperature, and are somewhat greater in N_2 than in air. © 2000 Elsevier Science Ltd. All rights reserved.

Keywords: Electrical resistance; Grain boundaries; Impedance spectroscopy; $SrTiO_3$

1. Introduction

The barrier character of grain boundaries of strontium titanate ceramics play an important role on low temperature applications such as multilayer capacitors.[1] This interest thus prompted investigations to separate the bulk and grain boundary contributions by comparing impedance spectra obtained for single crystals, bicrystals, and ceramic samples,[2,3] this confirmed that the overall behaviour of ceramic samples may be affected by resistive grain boundaries, and that the grain boundary resistance may exceed the bulk resistance. However, the activation energy of the bulk conductivity is usually smaller than for the grain boundaries, and in this case one may still ignore the grain boundary contribution at sufficiently high temperatures. Therefore, high temperature conductivity measurements (typically above 800°C) often ignore the grain boundary contribution.[4–6]

The relaxation time of the grain boundary contribution is usually several orders of magnitude larger than for the bulk contribution, and one may thus be able to separate the bulk and grain boundary contributions.[7–9] Denk and co-authors[7] ascribed the bulk and grain boundary contributions by comparing the impedance spectra obtained for single crystals and bicrystals. The electrode contributions may be identified by superimposing a dc bias, and/or on comparing impedance spectra obtained with different electrodes.

Investigations of the grain boundary and electrode contributions of $Zr_{1-x}Y_xO_{2-x/2}$, or $Zr_{1-x}Ca_xO_{2-x}$ electrolytes.[10–17] may also contribute to improve our understanding of the grain boundary properties of titanates. For example, the grain boundary resistance is expected to increase with decreasing grain size[17] but much greater effects were ascribed to the segregation of impurities (e.g. SiO_2 in ZrO_2-based materials),[11] or even formation of a liquid phase.[13,14] Cosegregation of impurities and one of the main additive (Ca or Y) has also been observed.[15,16]

The grain boundary resistance R_{gb} is expected to increase with increasing number of boundaries across the sample, and on assuming a simple brick layer model[17] this becomes $R_{gb} = \rho_{gb}\delta_{gb}N_{gb}/A$, or

$$R_{gb}d_gA/L = \rho_{gb}\delta_{gb} \quad (1)$$

where ρ_{gb} is the grain boundary resistivity, δ_{gb} is the grain boundary thickness, $N_{gb} = L/d_g$ is the number of grain boundaries across the sample, L is the sample thickness, A is the electrode area, and d_g is the average

* Corresponding author. Tel.: +351-34-370254; fax: +351-34-25300.
E-mail address: jfrade@cv.ua.pt (J.R. Frade).

PII: S0955-2219(00)00022-4

grain size. One may assume similar values of grain boundary thickness δ_{gb} for every sample, in which case $R_{gb}d_gA/L$ should be nearly independent of the grain size of the samples. The applicability of the brick layer model might thus be assessed by checking if data obtained for different samples obey a common dependence of $\ln(R_{gb}d_gL/A)$ versus $1/T$.

One may also predict a trend for the effects of grain size on the grain boundary capacitance, on assuming that the effective thickness is given by $\delta_{gb}N_{gb} = \delta_{gb}L/d_g$. In this case $C_{gb} = \varepsilon_o\varepsilon_r Ad_g/(\delta_{gb}L)$, where ε_o is the permitivity of vacuum, and ε_r the dielectric constant. One may thus account for the effects of grain size by plotting

$$C_{gb}L/(Ad_g) = \varepsilon_o\varepsilon_r/\delta_{gb} \quad (2)$$

versus temperature. The values of $\varepsilon_o\varepsilon_r/\delta_{gb}$ should also be nearly independent of the grain size.

Fleig and Maier[18] predicted that some microstructural features might exert additional effects on the impedance spectra, thus causing deviations from the brick layer model. For example, such a deviation was predicted for a bimodal distribution of small and large grains because the current lines might make detours across the largest grains to minimise the number of boundaries effectively crossed. Such effects might also be responsible for differences between the true activation energy of the grain boundary resistivity, and the value extracted from the temperature dependence of the grain boundary resistance (R_{gb}) obtained by fitting the impedance spectra.

The present work reports experimental results to assess the validity of the brick layer model in $SrTiO_3$ polycrystals with different microstructures. The microstructure of one of the samples shows a distribution of large and small grain sizes, to assess if this yields impedance spectra with unusual features.

2. Experimental procedure

Powders of undoped $SrTiO_3$ were prepared by powder reactions of $SrCO_3$ (BDH30275) and TiO_2 (Merck808). These reactants were mixed for 2 h in a nylon container, with zirconia balls and ethanol, then dried and calcined at 1100°C for 15 h. The calcined product was then milled again to enhance the homogeneity, and to destroy the agglomerates, and the resulting powders were used to obtain pellets for the electrical measurements. These pellets were uniaxially pressed and fired in different conditions to obtain differences in average grain size and/or in grain size distributions (Table 1).

Every sintered sample was polished and thermally etched for 30 min at a temperature which was 10% below the corresponding sintering temperature (°C).

Table 1
Firing temperature (T), and time (t), and the corresponding average grain size (d_g) of the samples

Sample	T (°C)	t (h)	d_g (μm)
ST1600	1600	20	31
ST1480	1480	20	11
ST1400	1400	4	3

The density was measured by immersion in Hg, and the lattice parameter was used to evaluate the theoretical density (5.14 g/cm^3). X-ray diffraction was used to confirm that every sample was single phase, and to calculate the lattice parameter.

Fig. 1 shows typical scanning electron micrographs obtained with the firing schedules presented in Table 1. These microstructures were image analysed to evaluate the grain size distributions (Fig. 2), and the corresponding average grain size (also shown in Table 1).

The HP4284A Precision LCR Meter was used to obtain impedance spectra in the temperature range 300 to 1000°C, with Pt electrodes. These measurements were performed both in air and N_2. A potentiometric oxygen sensor was used to evaluate the oxygen partial pressure in the N_2 atmosphere.

3. Results and discussion

The impedance spectra of samples ST1400, ST1480, and ST1600 in air are shown in Figs. 3–5. These spectra are nearly described by a series association of RC elements. The largest component of the spectra is usually a depressed arc, in which case the capacitance must be replaced by a constant phase element (CPE), as shown in Fig. 6. A code developed by Boukamp[19] was used to extract the relevant fitting parameters.

The resistance of the high frequency contribution is nearly independent of the average grain size, and was thus ascribed to the bulk (or grain interiors). The values of bulk resistance R_B were used to obtain the bulk conductivity $\sigma_B = L/(R_BA)$ shown in Fig. 7. The temperature dependence of the bulk conductivity in air yields an activation energy of 0.99 eV, which is close to the values reported for the p-type behaviour of undoped and stoichiometric strontium titanate,[2] and acceptor-doped strontium titanate.[8]

The values of bulk capacitance, and the corresponding permitivity (Fig. 8) are nearly independent of the average grain size, and are also nearly independent of temperature, as expected for strontium titanate materials.[8] The order of magnitude of our values also agrees with those reported by Vollmann and Waser.[8]

The bulk resistance was used to adjust the scales in the impedance spectra (Figs. 3–5), and to reveal the differences between the bulk and the remaining contributions.

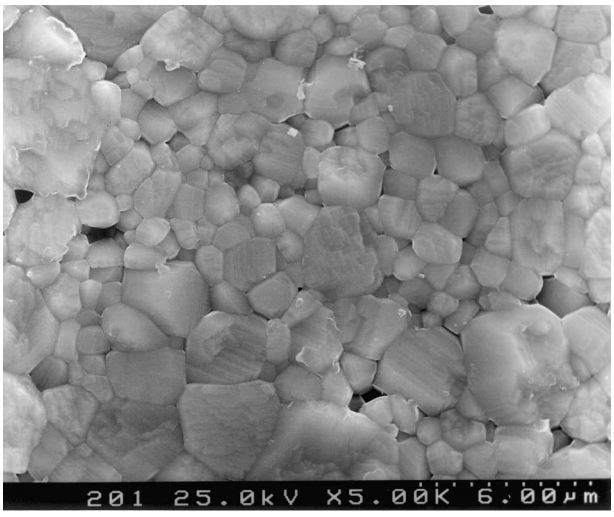

(a)

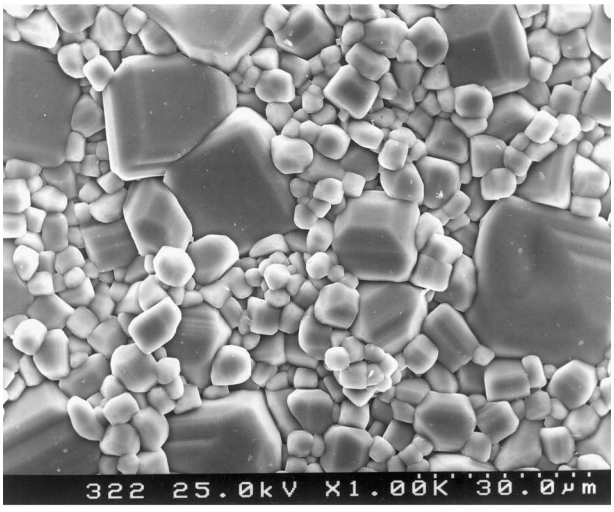

(b)

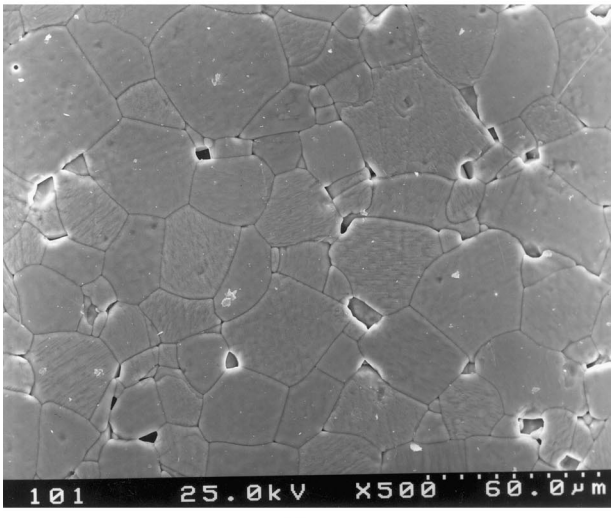

(c)

Fig. 1. Scanning electron microstructures of samples ST1400, ST1480, and ST1600 sintered in conditions shown in Table 1.

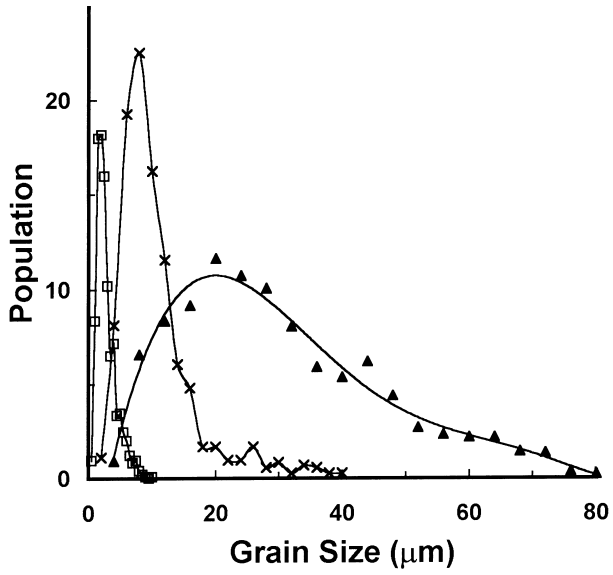

Fig. 2. Grain size distributions of samples ST1400 (□), ST1480 (×), and ST1600 (▲).

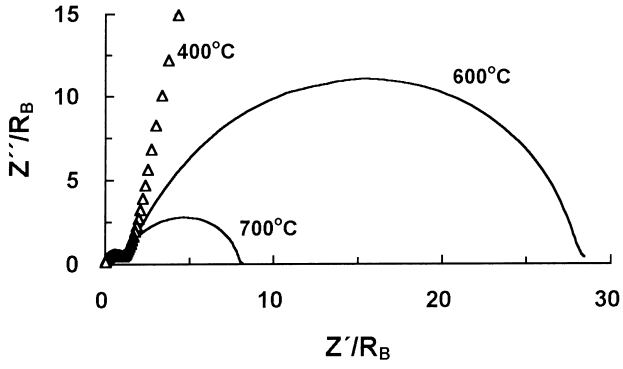

Fig. 3. Normalized impedance spectra of sample ST1400 in air, at 400, 600, and 700°C, with the corresponding values of $R_BS/L = 44.4$, 0.665, and 0.318 kΩ m.

The largest arc of most Nyquist plots depends on the actual grain size and was thus ascribed to the grain boundaries. The effects on the grain boundary resistance (Fig. 9) are consistent with the trend predicted for the brick layer model [Eq. (1)], and the corresponding activation energy (≈1.47 eV in air) is close to typical values reported for the grain boundary conductivity of acceptor-doped materials.[7] The value reported for Ni-doped samples[8,9] in the high temperature range is close to $W_g/2 \approx 1.6$ eV, where W_g denotes the bandgap.

The values of pseudocapacitance obtained on assuming a constant phase element for depressed grain boundary arcs may differ significantly from the true capacitance. The values of grain boundary capacitance were thus obtained on combining the grain boundary resistance and the peak frequency as follows:

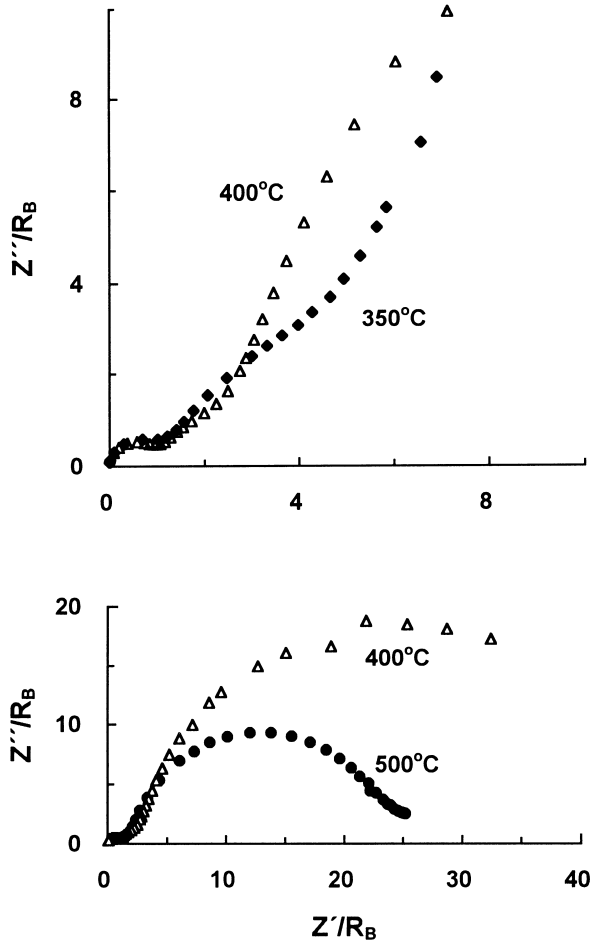

Fig. 4. Normalized impedance spectra of sample ST1480 in air, at 350, 400, and 500°C, with the corresponding values of $R_B S/L = 89$, 23.7, and 2.48 kΩ m.

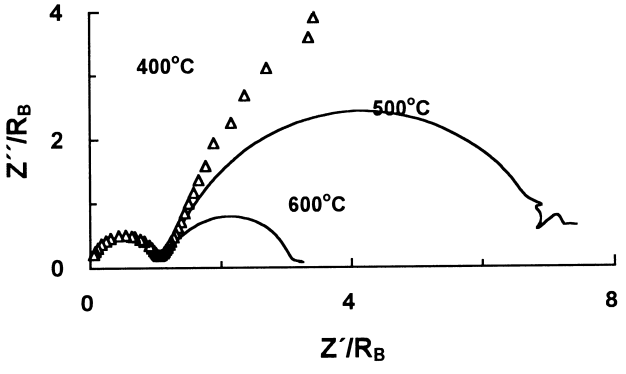

Fig. 5. Normalized impedance spectra of sample ST1600 in air, at 400, 500, and 600°C, with the corresponding values of $R_B S/L = 28.5$, 2.47, and 0.542 kΩ m.

$$C_{gb} = \left(2\pi f_{gb} R_{gb}\right)^{-1}. \quad (3)$$

These values increase with the average grain size, with typical values of $C_{gb}L/A$ in the order of 1.5 μF/m for sample ST1600, 0.5 μF/m for sample ST1480, and 0.15 μF/m for sample ST1400. These differences are nearly

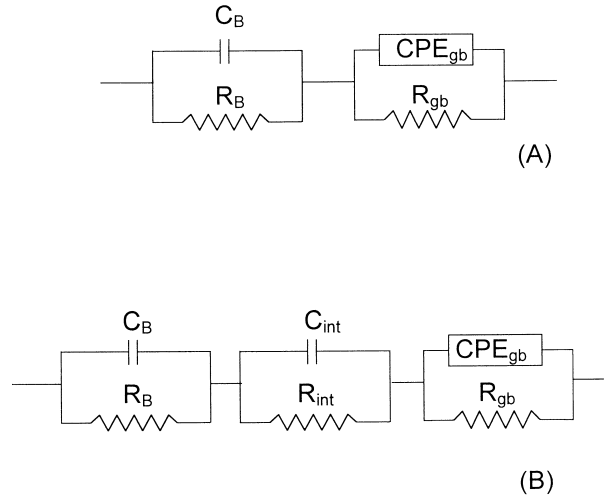

Fig. 6. Equivalent circuit proposed for strontium titanate samples (A), and an alternative circuit for sample ST1480 in air.

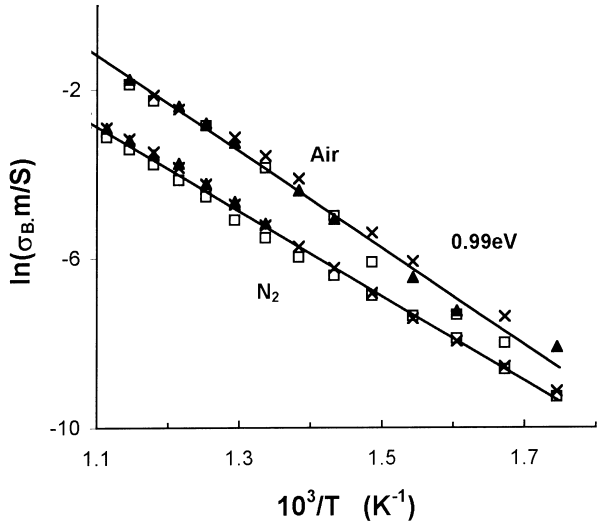

Fig. 7. Bulk conductivity of samples ST1400 (□), ST1480 (×), and ST1600 (▲), in air (upper values), and in N_2 (lower values).

accounted for by the differences in average grain size of the samples (Table 1), as predicted by Eq. (2) One should thus expect a common trend for samples with different grain sizes on resorting to the representation shown in Fig. 10. The remaining differences between the samples are close to the order of magnitude of experimental errors. Note that estimates of capacitance (extracted by fitting impedance spectra) sometimes involve errors of up to 50%.

The impedance spectra obtained for sample ST1480 (Fig. 4) show an unexpected additional shoulder on the left of the grain boundary arc, especially at temperatures below about 400°C. This shoulder may be accounted for by assuming an additional $R_{int}C_{int}$ term with a typical relaxation frequency in the intermediate range, and the equivalent circuit shown in Fig. 6B. The

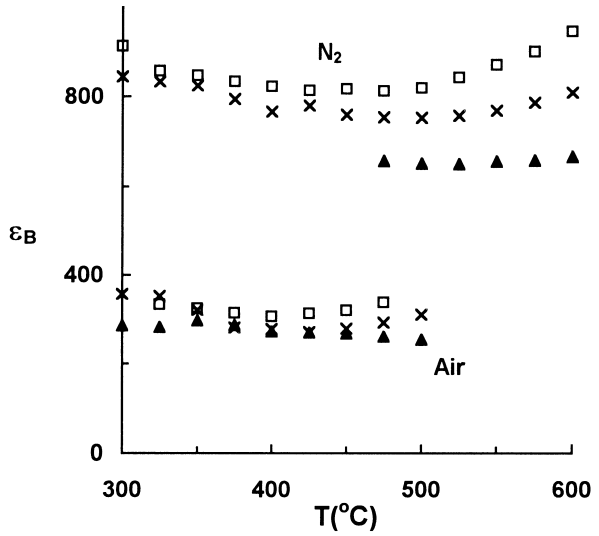

Fig. 8. Values of bulk dielectric constant $\varepsilon_B = C_B L/A\varepsilon_o$ of samples ST1400 (□), ST1480 (×), and ST1600 (▲), in air (lower values), and in N_2 (upper values).

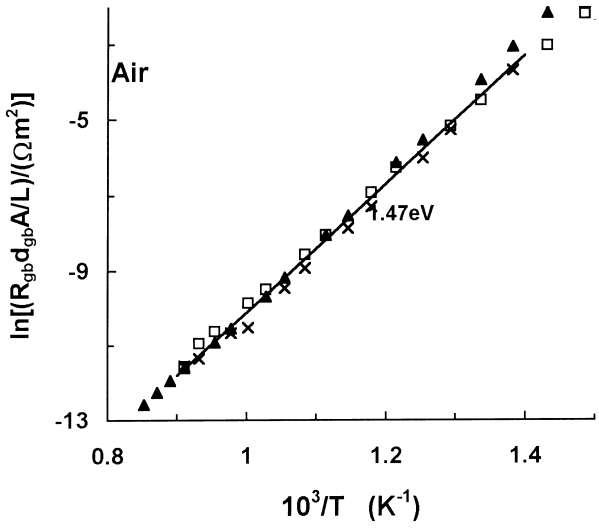

Fig. 9. Temperature dependence of the grain boundary resistance of samples ST1400 (□), ST1480 (×), and ST1600 (▲), in air, with corrections for differences in area to thickness ratio (A:L), and differences in average grain size d_g.

relevant fitting parameters are shown in Table 2, for selected temperatures.

Fleig and Maier[18] also predicted a similar shoulder on the left side of the grain boundary arc for samples with unusual microstructures. However those features are quite different from the nearly bimodal size distribution of our sample ST1480. In a separate article,[20] Fleig and Maier showed that current detours in microstructures with bimodal size distributions are likely to lower the grain boundary resistance (relative to the brick layer model). These simulated cases did not show asymmetric grain boundary arcs, except possibly for cases with two types of grain boundaries with significantly different properties.

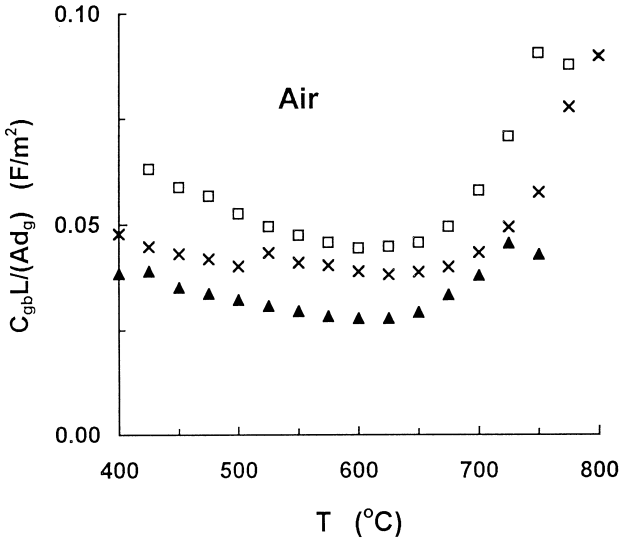

Fig. 10. Grain boundary capacitance of samples ST1400 (□), ST1480 (×), and ST1600 (▲), in air, with corrections for differences in thickness to area ratio (L:A), and differences in average grain size d_g.

Table 2
Fitting parameters obtained from spectra of sample ST1480 with the equivalent circuit shown in Fig. 6B

	T=400°C	T=450°C	T=500°C
R_B (kΩ)	23.7	6.6	2.48
R_{int} (kΩ)	26.1	5.8	1.74
R_{gb} (kΩ)	1130	225	57
C_B (pF)	22.1	22.2	24.8
C_{int} (nF)	0.69	0.70	0.80
C_{gb} (nF)	11.1	11.5	13.3
n	0.843	0.862	0.860

The spectra obtained for sample ST1480 in N_2 (Fig. 11) do not show the additional shoulder, thus raising additional doubts about its interpretation. In order to clarify these differences one also obtained a complete set of impedance spectra both in air and in N_2, to assess if this may be due to significant changes in the relative role of the bulk and grain boundary contributions (e.g. differences between the values of σ_B/σ_{gb} in N_2 and in air, changes in bulk and/or grain boundary capacitances, etc.).

The relevant parameters extracted from the impedance spectra (Figs. 12 and 13) indicate that the relative differences between the bulk and grain boundary relaxation frequencies are greater in air than in N_2. For example, the values of the frequency ratio f_B/f_{gb} extracted from the spectra in air, (about 10^4 at 400°C, and 9×10^3 at 450°C), are higher than the values extracted from impedance spectra in N_2 ($f_B/f_{gb}=5\times10^3$ at 450°C, 3×10^3 at 500°C, and 1.4×10^3 at 550°C). In this type of condition the spectra obtained in air should show slightly better separation of the bulk and grain boundary contributions, enhancing the possibility of detecting an additional contribution with an intermediate frequency f_{int}

in the range $f_{gb} \leqslant f_{int} \leqslant f_B$. The shoulder shown in Fig. 4A is thus likely to correspond to a genuine relaxation process rather than an artifact typical of irregular microstructures. For example, a slight deviation from the stoichiometric composition might promote liquid phase formation above the eutectic temperature in the system $SrTiO_3$–TiO_2, as suggested by Cho and Johnson.[21] Note also that liquid phase formation might be responsible for the onset of grain growth shown by the microstructure of sample ST1480 (Fig. 1).

Computer simulations[18] also showed that the deviations from the brick layer model should be minimised on lowering the bulk to grain boundary conductivity ratio σ_B/σ_{gb}, thus contributing to attain a better separation of the bulk and grain boundary elements. For example, current detours across large grains may effect the total grain boundary resistance of materials with a bimodal size distribution, especially for cases when the bulk conductivity is much higher than the conductivity of grain boundaries. The actual results suggest that the conductivity ratio σ_B/σ_{gb} is lower in air than in N_2, and the deviations from the brick layer model should also be lower in air. In fact, the changes in conductivity ratio can be evaluated from the resistance ratio $R_{gb}/R_B = (\delta_{gb}/d_g)(\sigma_B/\sigma_{gb})$ or

$$d_g(R_{gb}/R_B) = \delta_{gb}(\sigma_B/\sigma_{gb})$$

The results in Fig. 14 thus show that the values of σ_B/σ_{gb} are lower in air than in N_2, and the deviations from the brick layer model should also be lower in air.

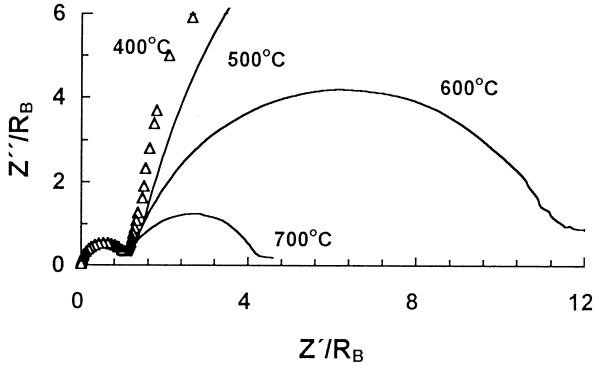

Fig. 11. Normalized impedance spectra of sample ST1480 in N_2, at 400, 500, 600, and 700°C, with the corresponding values of $R_BS/L = 91$, 10.4, and 2.43 kΩ m.

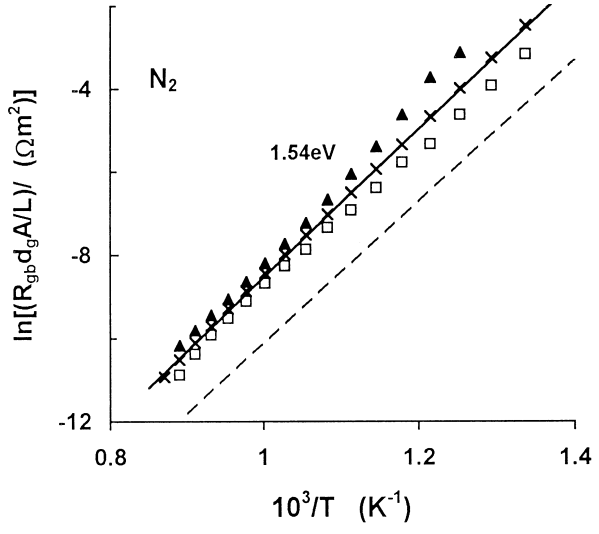

Fig. 12. Temperature dependence of the grain boundary resistance of samples ST1400 (□), ST1480 (×), and ST1600 (▲), in N_2, with corrections for differences in area to thickness ratio (A:L), and differences in average grain size d_{gb}. The dashed line represents the overall trend for the results in air (shown in Fig. 9).

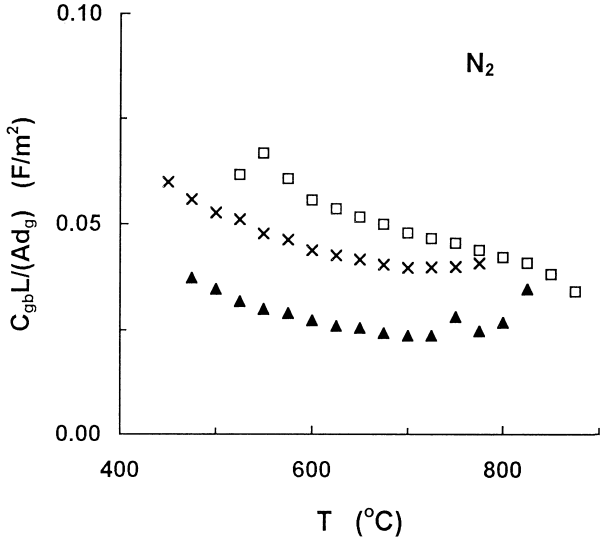

Fig. 13. Grain boundary capacity of samples ST1400 (□), ST1480 (×), and ST1600 (▲), in N_2, with corrections for differences in thickness to area ratio (L:A), and differences in average grain size d_g.

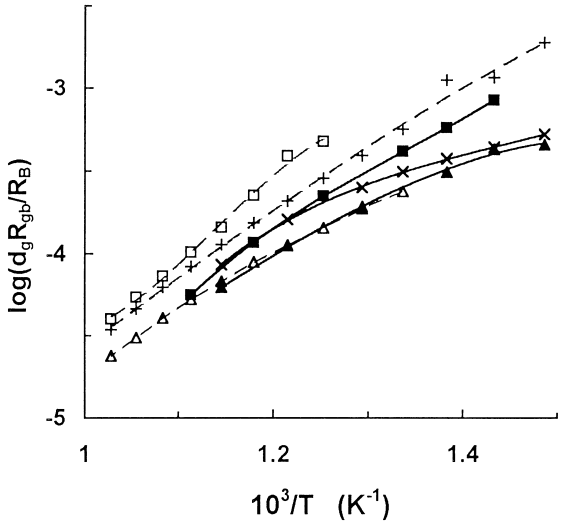

Fig. 14. Changes in grain boundary to bulk resistance ratio of samples ST1400 (squares), ST1480 (circles), and ST1600 (triangles), in air (solid lines), and in N_2 (dashed lines).

The conductivity ratio σ_B/σ_{gb} increases with decreasing temperature, due to the difference between the activation energies of the bulk and grain boundary conductivities; this also explains the increasing deviations from the brick layer model with decreasing temperature (Figs. 9, 12, 13), especially in N_2. Note that the representation of $R_{gb}d_gA/L$ should yield nearly identical results for every sample. A comparison between the data shown in Figs. 9 and 12 thus suggests that the results in air are closer to the brick layer model, and it might thus be easier to observe the onset of an additional intermediate term with a relaxation frequency in the range $f_{gb} < f_{int} < f_B$.

4. Conclusions

The effects of grain size on the values of grain boundary resistance and capacity extracted from impedance spectra nearly agree with typical trends predicted on assuming a brick layer model. However, the deviations from this brick layer model tend to increase with decreasing temperature, possibly because the bulk to grain boundary conductivity ratio σ_B/σ_{gb} increases on cooling. Slight differences between air and moderately reducing conditions (N_2) might also be related to differences in σ_B/σ_{gb}. The impedance spectra obtained for a sample with a nearly bimodal size distribution show an additional intermediate contribution in air but one could not find a clear relation between this and the relevant microstructural features. The corresponding spectra in moderately reducing conditions (N_2) did not show the intermediate term.

Acknowledgements

This work was supported by the Portuguese Foundation for Science and Technology (FCT), under Contract PRAXIS XXI 3/3.1/MMA/1760/95, and by the European Commission under a network research contract FMRX-CT97-0130.

References

1. Yamaoka, N. and Matsui, T., Properties of $SrTiO_3$-based boundary layer capacitors. In *Advances in Ceramics, Vol. I, Grain Boundary Phenomena in Electronic Ceramics*, ed. L. M. Levinson and D. C. Hill. American Ceramic Society, Columbus, OH, 1981, pp. 232–241.
2. Walters, L. C. and Grace, R. E., Formation of point defects in strontium titanate. *J. Phys. Chem. Solids*, 1967, **28**, 239–244.
3. Denk, I., Munch, W. and Maier, J., Partial conductivities in $SrTiO_3$: Polarization experiments, oxygen concentration cell measurements, and defect chemistry modelling. *J. Am. Ceram. Soc.*, 1995, **78**, 3265–3272.
4. Balachandran, U. and Eror, N. G., Electrical conductivity of strontium titanate. *J. Solid State Chem.*, 1981, **39**, 351–359.
5. Chan, N. H., Sharma, R. K. and Smyth, D. M., Non-stoichiometry in $SrTiO_3$. *J. Electrochem. Soc.*, 1981, **128**, 1762–1769.
6. Moos, R. and Hardtl, K. H., Dependence of the intrinsic conductivity minimum of $SrTiO_3$ ceramics on the sintering atmosphere. *J. Am. Ceram. Soc.*, 1995, **78**, 2569–2571.
7. Denk, I., Claus, J. and Maier, J., Electrochemical investigations of $SrTiO_3$ boundaries. *J. Electrochem. Soc.*, 1997, **144**, 3526–3535.
8. Vollman, M. and Waser, R., Grain boundary defect chemistry of acceptor doped titanates: Space charge layer width. *J. Am. Ceram. Soc.*, 1994, **77**, 235–243.
9. Vollman, M., Hagenbeck, R. and Waser, R., Grain boundary defect chemistry of acceptor doped titanates: Inversion layer and low field conduction. *J. Am. Ceram. Soc.*, 1997, **80**, 2301–2314.
10. Bauerle, J. E., Study of solid electrolyte polatization by a complex admittance method. *J. Phys. Chem. Solids*, 1969, **30**, 2657–2670.
11. Verkerk, M. J., Middelhius, B. J. and Burggraaf, A. J., Effect of grain boundaries on the conductivity of high purity ZrO_2–Y_2O_3 ceramics. *Solid State Ionics*, 1982, **6**, 159–170.
12. Badwal, S. P. S. and Drennan, J., Yttria–zirconia: effect of microstructure on conductivity. *J. Mat. Sci.*, 1987, **22**, 3231–3239.
13. Godickemeier, M., Michel, B., Orlinkas, A., Bohac, P., Sazaki, K., Gaukler, L., Heinrich, H., Schwander, P., Kostorz, G., Hofmann, H. and Frei, O., Effect of intergranular glass films on the electrical conductivity of 3Y-TZP. *J. Mat. Res.*, 1990, **9**, 1228–1240.
14. Boutz, M. M. R., Chen, C. S., Winnubst, L. and Burggraaf, A. J., Characterization of grain boundaries in superplastically deformed Y-TZP ceramics. *J. Am. Ceram. Soc.*, 1994, **77**, 632–640.
15. Hwang, S. L. and Chen, I. W., Grain size control of tetragonal zirconia polycrystals using the space charge concept. *J. Am. Ceram. Soc.*, 1990, **73**, 3269–3277.
16. Aoki, M., Chiang, Y. M., Kosacki, I., Lee, L. J. R., Tuller, H. and Liu, Y., Solute segregation and grain boundary impedance in high purity stabilized zirconia. *J. Am. Ceram. Soc.*, 1996, **79**, 1169–1180.
17. Van Dijk, T. and Burggraaf, A. J., Grain boundary effects on ionic conductivity in ceramics. *Phys. Stat. Sol. A*, 1981, **63**, 229.
18. Fleig, J. and Maier, J., A finite element study on the grain boundary impedance of different microstructures. *J. Electrochem. Soc.*, 1998, **145**, 2081–2089.
19. Boukamp, B., A nonlinear squares fit procedure for analysis of immitance data of electrochemical systems. *Solid State Ionics*, 1986, **20**, 31–44.
20. Fleig, J. and Maier, J., The impedance of ceramics with highly resistive grain boundaries: Validity and limits of the brick layer model. *J. Eur. Ceram. Soc.*, 1999, **19**, 693–696.
21. Cho, S. G. and Johnson, P. F., Evolution of the microstructure of undoped and Nb-doped $SrTiO_3$. *J. Mat. Sci.*, 1994, **29**, 4866–4874.